Investigation of acoustic streaming and cavitation intensity in water as an analogue for liquid metal

[1,5] Iakovos Tzanakis*; [2]G. S. Bruno Lebon; [2,3]Dmitry Eskin; [4]Martin Hyde, [5]Patrick S. Grant

[1]Oxford Brookes University, Oxford, UK; [2]Brunel University London, Uxbridge, UK; [3]Tomsk State University, Tomsk, Russia; [4]TSI Instruments, UK; [5]University of Oxford, Oxford, UK

Abstract

This paper presents an investigation of the evolution of flow structures and cavitation intensity in water as an analogue for a liquid metal under ultrasonic excitation. Results are presented for 20 kHz high-power ultrasound. The input power ranged from 50% (8.5 μm p-p) to 100% (17 μm p-p). To identify the streaming structures and understand the recirculation flows for different vibrational amplitudes of the sonotrode, particle image velocimetry (PIV) measured the velocity field. Simultaneously, a calibrated cavitometer probe measured acoustic intensity in the fluid. The cavitation intensity away from the acoustic source decreased with increasing input acoustic power, but was relatively constant inside the cavitation zone (irrespective of the input power). PIV measurements showed that the direction of the flow pattern was strongly related to the vibrational amplitude of the sonotrode. These results are compared with the predictions of an acoustic cavitation model. The outcome of the present work will help to determine the efficient optimization of ultrasonic processing of liquid metals that is of increasing technological importance.

Keywords: Particle Image Velocimetry (PIV); acoustic streaming; cavitation intensity, ultrasonic melt processing, aluminium

Introduction

Ultrasonic melt treatment (UST) is an environment friendly and economical alternative to many conventional melt processes used to control liquid metal quality, such as fluxing, modification, and gas lancing. UST involves introducing high-intensity ultrasonic waves into liquid metal to induce acoustic cavitation [1]. Cavitation bubbles expand non-linearly, become unstable upon reaching a critical size, and collapse catastrophically, thereby generating high-speed liquid jets, shockwaves, and local hot spots [2–4]. Laboratory tests showed that UST offers beneficial effects, such as accelerated diffusion, activation of inclusions, improved wetting, dissolution, deagglomeration, and dispersion of particles leading to degassing, refined, equiaxed solidification microstructure, and uniform distribution of constituent phases [5–9]. However, an insufficient understanding of the phenomena governing UST (e.g. cavitation intensity distribution and acoustic streaming) hinders more widespread implementation of UST technology in industry [10].

The understanding and quantification of recirculation patterns within the acoustic cavitation zone and the mass exchange between the cavitation zone and the surrounding fluid are important for optimizing UST e.g. for the grain refinement of the as-cast structure. Recently, Wang *et al.* [11] showed that a continuous recirculation pattern created a low temperature gradient throughout the melt: this favours an equiaxed grain structure, which is usually preferred by industry. In direct-chill casting, induced-acoustic streaming promotes forced convection that is opposed and much stronger to natural convection in the melt, facilitating further activation (wetting) of extrinsic particles, solid fragmentation and self-grain refining, mixing and elemental homogenisation within the bulk melt [5].

So far, no accurate comprehensive theory of acoustic streaming with cavitation has been developed. There were some successful attempts to model acoustic streaming using a sonotrode as a flow/pressure source and getting average distribution of velocities [12,13] as well as performing PIV measurements of acoustic flows generated by a sonotrode[13,14]. The calculated range of velocities was between 0.2 and 2 m/s [12] while PIV measurements gave the range up to 0.1 m/s [13] for similar ultrasonic conditions. Linking the intensity and details of cavitation to acoustic streaming in modelling approaches remains a major challenge. Barthès *et al.* [14] used PIV techniques to demonstrate the interaction between the acoustic streaming below a sonotrode with a transverse horizontal flow in a rectangular duct, showing that cavitation bubbles can be transported significant distances by the flow and remain active, which may be important for practical applications [15]. To get more insight into the inter-related effects of cavitation and acoustic streaming, a combination of visualisation techniques and simultaneous acoustic measurements, and more sophisticated modelling, is required.

* Corresponding Author, Iakovos Tzanakis: itzanakis@brookes.ac.uk

In this study, we use a calibrated cavitometer [16] to characterise cavitation development in water and PIV to study acoustic streaming inside and near the cavitation zone. Experiments were performed in water because it is both a convenient and suitable analogue (among the range of possible transparent liquids) to molten aluminium in studies of acoustic cavitation [17].

Methodology

A Hielscher 20-kHz ultrasonic transducer introduced continuous acoustic waves in a rectangular, glass tank of base area 300 mm × 200 mm filled with distilled water (Figure 1). The liquid height was 150 mm and the radiating surface (radius 20 mm) of the vertically mounted titanium sonotrode was immersed 20 mm below the liquid surface. Acoustic power was initially at 50% and was gradually increased to 100%. The amplitude of the vibrating surface at 100% power was 17 µm peak-to-peak. A wattmeter was integrated to the transducer device to record power. The acoustic power of the sonotrode was obtained by subtracting the input electric power of the transducer when the sonotrode operated in the studied liquid from that measured in air, the reference medium. The acoustic power of the sonotrode was 90±3 Watt when operating at 100% power. The temperature was continuously monitored during the experiments and was maintained at 21±1 °C.

Cavitation intensity measurements were taken with a cavitometer probe in different positions, along the z-axis (Figure 1). Measurements between the sonotrode and the sidewall of the tank were taken at 6 different points of interest: under the sonotrode and at 5, 7, 9, 11 and 13 cm from the sonotrode centre-point. The cavitometer probe had a spatial resolution of about ~50 mm, allowing measurements of acoustic intensities of frequency components up to 10 MHz. The 4 mm waveguide of the cavitometer probe was submerged to a depth of 80 ± 2 mm. A full account of the cavitometer design and performance can be found elsewhere [16].

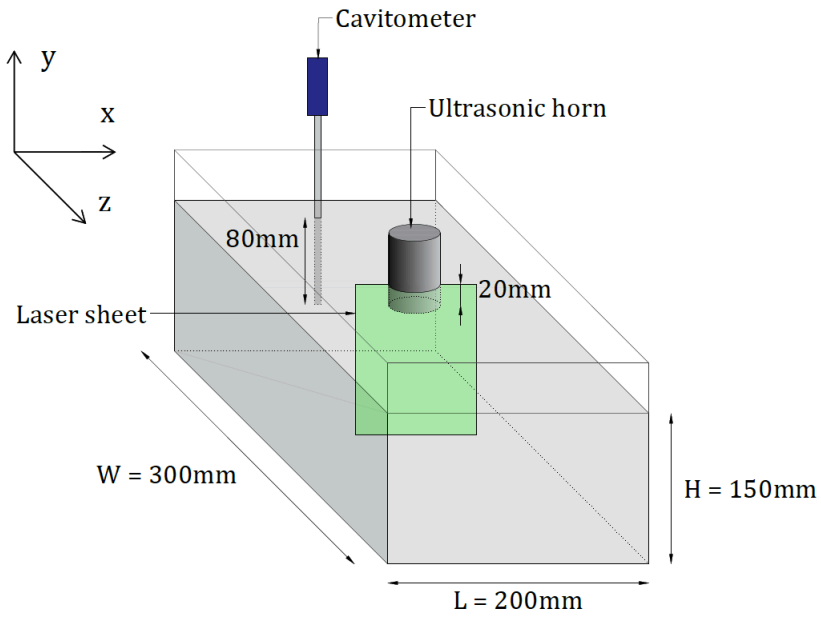

Figure 1: Graphical representation of the experimental test rig for measuring cavitation intensity and acoustic streaming

A TSI particle image velocimetry (PIV) system measured acoustic streaming velocities along the cavitation zone and in the bulk volume. A dual cavity Nd YAG laser source – wavelength 532 nm – generated a ≈1 mm thick 2D pulsed-laser sheet. A short time interval Δt separated the two pulses; Δt was set at 250 µs or 500 µs, depending on the operating conditions. For each operating condition, a set of 100 pairs of images was captured using a TSI PowerView 4MP-LS digital CCD camera with an array of 2352 by 1768 pixels and a 50mm F1.8 Nikon lens operated at a maximum frame rate of up 16 frames per second and positioned normal to the illuminated plane. The PowerView 4MP-LS camera utilised frame straddling to enable short inter-frame times. Glass hollow sphere seeded particles (≈10 µm in diameter) with density close to water were added at a concentration such that 5–10 particles were recorded in each frame and typically 5 pair of images were recorded per second. Acoustic streaming measurements were initiated by positioning the acoustic propagation axis within the laser sheet with measurements taken in the plane $z = 0$ (Figure 1) with the origin at the radiating surface centre. With the particles in the illuminated plane in focus, the resultant x-y field of view was 85 mm × 95 mm. Using TSI's Insights software, an interrogation area of 64 x 64 pixels with 50% overlap was set, and the same software used for PIV analysis and the production of 2D time-averaged vector flow fields.

Results and Analysis

Cavitation Intensity Measurements. To characterise cavitation development, a series of acoustic measurements using a calibrated cavitometer were performed across the experimental tank. As expected, the cavitation spectrum consisted of acoustic emissions from the fundamental frequency and emissions from the collapsing bubbles that were strongly dependent on the acoustic power and the distance from the source.

Figure 2 shows a range of measured cavitation intensity values: at distances of 5 cm, 7 cm and 9 cm from the sonotrode axis. The cavitation intensity gradually decreased with acoustic power up to a point (around 80–90% of the maximum) where it rebounded in magnitude. At longer distances, the intensity continuously reduced across the acoustic power range because of the shielding and scattering effects commonly generated in sonicated environments. As the sonotrode power increased, the number of the bubbles below the horn also increased, hindering sound wave propagation into the bulk liquid. Concomitantly, neighbouring bubbles shielded bubbles inside the bubbly cloud to some extent, inhibiting their growth. Upon collapse, these interior bubbles produced less powerful impact pressures in contrast to the fully developed (based on the fundamental frequency [17]) cavitation bubbles. Consequently, weaker acoustic waves reached the cavitometer probe [18]. At a higher power of 100%, acoustic streaming pushed the bubbly clouds away and a cone-like bubbly structure was formed, facilitating the propagation of the cavitation and acoustic waves to the liquid. Hence, the overall cavitation intensity increased. Nevertheless, the intensity remained approximately 20% lower than that measured at 50% power.

Under the sonotrode, the largest intensity was measured at 100%, with an approximately linear relationship between cavitation intensity and acoustic power (see plot "under" in Figure 2). However, at 80% power there was a drop in intensity and deviation from this trend. This is likely attributed to the shielding effects as explained in [16]. A further increase followed as with more power acoustic streaming pushed the accumulated bubbly structures further apart and released the pathway for sound wave propagation. This highlighted the inter-related role of the cavitation zone and bubbly structures in regulating acoustic pressure propagation.

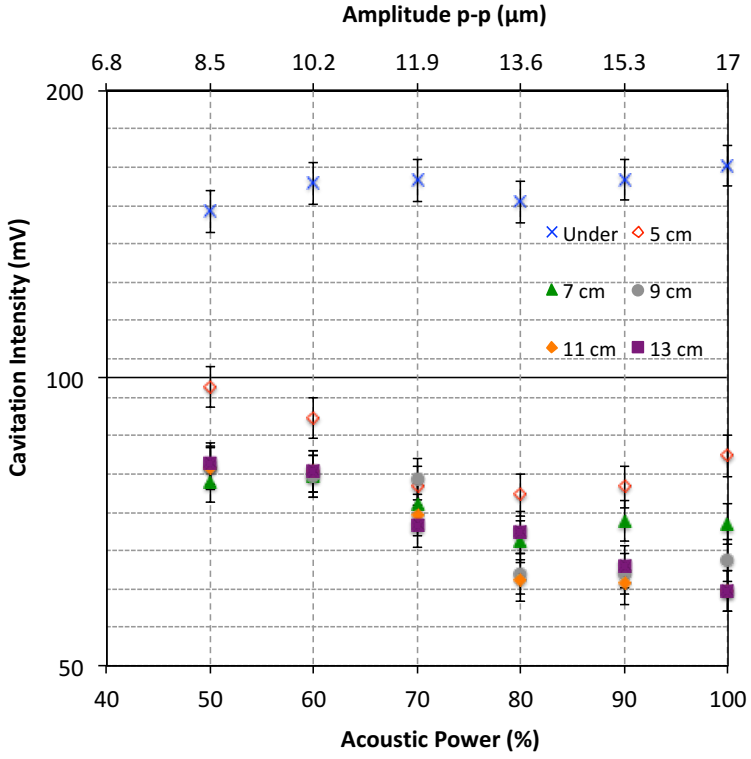

Figure 2: The cavitation intensity measured by a cavitometer versus the acoustic power from the 20 kHz transducer. Peak to peak displacements of the tip of the sonotrode in relation to the acoustic power are also shown.

Interestingly, for all other cases away from the cavitation zone, the 50% power produced the most efficient cavitation activity. At 50%, fewest bubbles were generated resulting in bubble displacement without excessive disruptions from other neighbouring bubbles. Bubble growth was comparatively smooth and not severely affected by the shielding effect. This effect was advantageous because the generation of the maximum

cavitation intensity occurred below 100% sonotrode power resulting in potential environmental and economic benefits for ultrasonic aided technologies.

Variation of the maximum intensity with the distance from the source is also depicted in Figure 2. The highest cavitation intensity measured by the cavitometer probe was near the sonotrode. In general, there was a reduction of about 25% as the measuring point moved from 5 cm to 13 cm and results are in a good agreement with [18,19] where a decay in intensity with distance from the source was also reported.

PIV Measurements. Figure 3 shows typical PIV measurements for the two extremes of the acoustic power range of 50% (left) and 100% (right). Each vector represents the time-averaged distribution of velocities, from 100 pair of images.

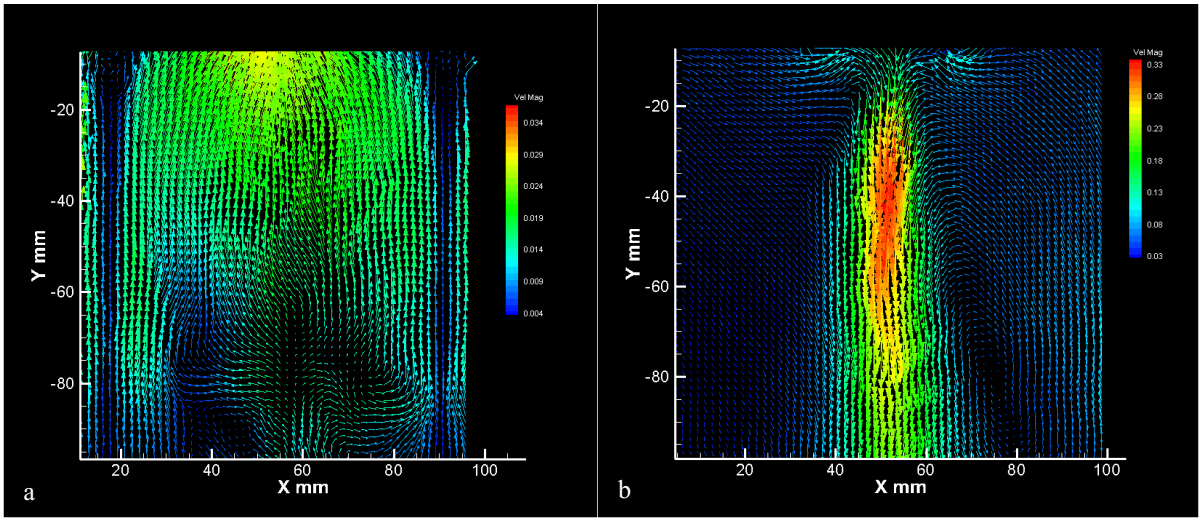

Figure 3: Typical images of PIV showing spatial distribution of acoustic flow structures under different input power at 50% (a, left) and 100% (b, right) acoustic power from the transducer. Legend: velocity magnitude in m/s (0.004–0.034 left, 0.03–0.33 right).

Acoustic streams at 50% power moved towards the horn and then recirculated, following the same pattern on either of the side of the sonotrode, as previously shown in [20]. In contrast, at 100 %, the flow had a distinct downward movement, with almost an order of magnitude increase in peak velocity, with comparatively weak recirculating patterns formed on both sides along the symmetry line of the acoustic stream, which is a typical streaming pattern [13]. Overall, the recirculation patterns and velocity magnitudes and directions were markedly different at the two power settings. From a technological viewpoint, the less intuitive – perhaps "unusual" – flow pattern (at 50%) may facilitate the application of ultrasound to liquid metals in the cavitation zone because the melt residence time in the cavitation zone is increased due to slower streams, while the "back flow" towards the horn continuously re-cycles a stream of melt into the cavitation zone. At the same time, the acoustic intensity is still high enough for effective treatment of the liquid volume (Figure 2). This flow behaviour was monitored across the tip of the sonotrode and repeated using differently positioned optical 2D slices to ensure the findings in Figure 3 were reproducible and representative.

Careful examination of the acoustic stream development on increasing the acoustic power from 50% to 100% suggested that the switch from upward to downward flow occurred at approximately 55% acoustic power. For a firmer conclusion of this transition, a higher temporal resolution in the PIV image pair acquisition would be helpful.

A possible interpretation for the predominantly "upward flow" at 50% power in Figure 3 is that the sound wave may penetrate the bubbly zone and establish a standing wave, creating bubble streams that may induce net upward flow, even if the sound radiation is propagating in the opposite direction. Thus this regime might be postulated as a "standing wave/stream filament" regime, as suggested in [21]. This may be similar to the behaviour of larger bubbles or bubbly clouds that can move against the flow towards the sonotrode tip, even when bulk flow moves in the opposite direction: Yasui *et al.* [22] used a 10 mm sonotrode with the same peak-to-peak amplitude used here (set at 8.5 μm) to show that some cavitation bubbles at distances of 1 cm or more from the horn tip moved toward the horn tip due to the secondary Bjerknes force acting on the bubbles near the horn tip. It is speculated that here a similar mechanism is dragging acoustic streams (flow and bubbles) towards the horn tip. At higher transducer powers, the shielding effect sets in and changes the wave from "standing" to

"traveling" via more efficient dissipation at the higher induced bubble density, in the immediate vicinity of the end of the horn, and net downwards acoustic streaming at a higher velocity dominates the flow.

At approximately 8 cm below from free surface at 50% power, acoustic streams bifurcated (Figure 3a) and there was both some upward flow towards the transducer but also more isotropic flow (at least in 2D). From a UST point of view, this reproducible phenomenon i.e. that within the same flow there are distinctive secondary multi-directional flows with dynamic recirculating flow patterns, together with strong eddies near the transducer and free surface under the same experimental conditions [20], may provide for a more efficient treatment of the liquid, even though velocity magnitudes are lower than at 100% power. This arises because flow paths are more varied and excessive recirculation (vortex) regions are avoided, helping to ensure macro-scale homogenisation of the liquid, noting that even at 50% power cavitation remains vigorous, as described in [23].

Numerical Modelling. In order to support the experimental insights, numerical modelling was investigated. The numerical model was based on the homogeneous cavitation model of Schnerr and Sauer [24] as implemented in the OpenFOAM solver *interPhaseChangeDyMFoam* [25], with turbulence handled using the kEqn LES model [26]. Numerical results were in broad qualitative agreement with the flow patterns at 100% acoustic power, but could not reproduce the reverse flow at 50% power, with reverse flow shown only very close to the sonotrode (Figure 4a). The pre-dominant downward flow (Figure 4b) at 100% power is well-explained by the net difference between the high pressure near the sonotrode and the lower pressures in regions away from the sonotrode, with the same overall trend pressure distributions at 50 % power (Figure 4a). The calculated flow velocity was higher than experiment at both acoustic powers, and was expected because a homogeneous cavitation model of the type used here for convenience cannot predict pressures (and therefore velocities) accurately at these high powers typical or technological applications. In future work, acoustic streaming will be integrated into a high-order acoustic model [19], and the present work underlines how some of the more convenient current modelling approaches cannot reproduce robustly experimental results at powers relevant to UST.

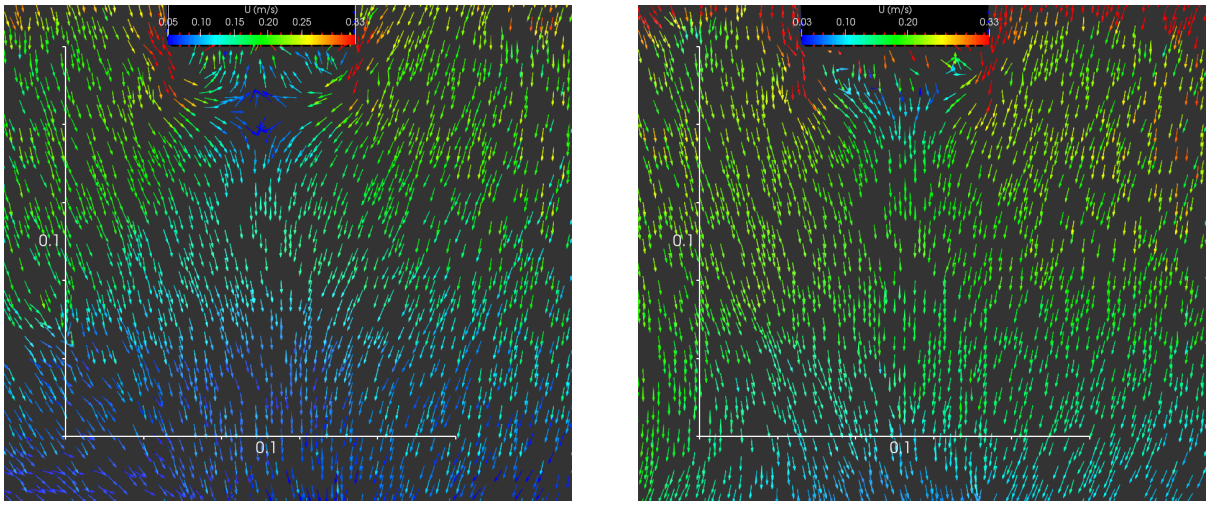

(a) (b)

Figure 4: Numerical prediction of flow pattern with (a) 50 % input power and (b) 100 % input power. The colour scale for velocity magnitude corresponds to scale in Figure 3 (b). The white axes delimit the corresponding field of view in the PIV measurements.

Conclusions

Experimental measurements showed that cavitation intensity in water used as a liquid metal analogue significantly reduced with increasing acoustic power away from the immediate vicinity of the sonotrode. PIV macro-scale measurements showed that flow velocity and direction were dependent on the operating power of the sonotrode transducer in a manner not captured by numerical modelling. Future numerical models need to better integrate microscopic cavitation, meso-scale bubble cloud dynamics and macro-scale acoustic streaming to reproduce better experimental behaviour. The approach described here of simultaneously investigating cavitation intensity distribution and acoustic streaming could be used to optimize the geometrical features of a casting arrangement and the liquid treatment efficiency in ultrasonic melt treatments. Looking further to the future, combining several transducers along the melt volume with variable acoustic power outputs, guided by improved modelling capability, could be used to flexibly generate a range of novel cavitation and flow regime combinations to optimize ultrasonic melt treatment.

Acknowledgements

Financial support from EPSRC (UK) under projects LiME Hub (EP/N007638/1), UltraMelt (EP/K00588X/1 and EP/K005804/1) and UltraMelt2 (EP/R011001/1, EP/R011044/1, EP/R011095/1) is gratefully acknowledged.

References

[1] Tzanakis, I., Lebon, G.S.B., Eskin, D.G., and Pericleous, K.A. (2016) *Characterisation of the ultrasonic acoustic spectrum and pressure field in aluminium melt with an advanced cavitometer*. J. Mater. Process. Technol., 229, 582–586.

[2] Xu, W.W., Tzanakis, I., Srirangam, P., Mirihanage, W.U., Eskin, D.G., Bodey, A.J., and Lee, P.D. (2016) *Synchrotron quantification of ultrasound cavitation and bubble dynamics in Al–10Cu melts*. Ultrason. Sonochem., 31, 355–361.

[3] Flannigan, D.J., and Suslick, K.S. (2005) *Plasma formation and temperature measurement during single-bubble cavitation*. Nature, 434 (7029), 52–55.

[4] Tzanakis, I., Eskin, D.G., Georgoulas, A., and Fytanidis, D.K. (2014) *Incubation pit analysis and calculation of the hydrodynamic impact pressure from the implosion of an acoustic cavitation bubble*. Ultrason. Sonochem., 21 (2), 866–878.

[5] Eskin, G.I., and Eskin, D.G. (2015) *Ultrasonic treatment of light alloy melts*, Taylor & Francis, CRC Press, Boca Raton.

[6] Tzanakis, I., Xu, W.W., Eskin, D.G., Lee, P.D., and Kotsovinos, N. (2015) *In situ observation and analysis of ultrasonic capillary effect in molten aluminium*. Ultrason. Sonochem., 27, 72–80.

[7] Atamanenko, T.V., Eskin, D.G., Zhang, L., and Katgerman, L. (2010) *Criteria of Grain Refinement Induced by Ultrasonic Melt Treatment of Aluminum Alloys Containing Zr and Ti*. Metall. Mater. Trans. A, 41 (8), 2056–2066.

[8] Eskin, D.G., Al-Helal, K., and Tzanakis, I. (2015) *Application of a plate sonotrode to ultrasonic degassing of aluminum melt: Acoustic measurements and feasibility study*. J. Mater. Process. Technol., 222, 148–154.

[9] Shu, D., Sun, B., Mi, J., and Grant, P.S. (2012) *A High-Speed Imaging and Modeling Study of Dendrite Fragmentation Caused by Ultrasonic Cavitation*. Metall. Mater. Trans. A, 43 (10), 3755–3766.

[10] Lebon, G.S.B., Tzanakis, I., Djambazov, G., Pericleous, K., and Eskin, D.G. (2017) *Numerical modelling of ultrasonic waves in a bubbly Newtonian liquid using a high-order acoustic cavitation model*. Ultrason. Sonochem., 37, 660–668.

[11] Wang, G., Croaker, P., Dargusch, M., McGuckin, D., and StJohn, D. (2017) *Simulation of convective flow and thermal conditions during ultrasonic treatment of an Al-2Cu alloy*. Comput. Mater. Sci., 134, 116–125.

[12] Trujillo, F.J., and Knoerzer, K. (2011) *A computational modeling approach of the jet-like acoustic streaming and heat generation induced by low frequency high power ultrasonic horn reactors*. Ultrason. Sonochem., 18 (6), 1263–1273.

[13] Schenker, M.C., Pourquié, M.J.B.M., Eskin, D.G., and Boersma, B.J. (2013) *PIV quantification of the flow induced by an ultrasonic horn and numerical modeling of the flow and related processing times*. Ultrason. Sonochem., 20 (1), 502–509.

[14] Barthès, M., Mazue, G., Bonnet, D., Viennet, R., Hihn, J.-Y., and Bailly, Y. (2015) *Characterization of the activity of ultrasound emitted in a perpendicular liquid flow using Particle Image Velocimetry (PIV) and electrochemical mass transfer measurements*. Ultrasonics, 59, 72–78.

[15] Tzanakis, I., Lebon, G.S.B., Eskin, D.G., and Pericleous, K. (2016) Optimization of the Ultrasonic Processing in a Melt Flow, in *Light Metals 2016* (eds.Williams, E.), Springer International Publishing, Cham, pp. 833–836.

[16] Tzanakis, I., Hodnett, M., Lebon, G.S.B., Dezhkunov, N., and Eskin, D.G. (2016) *Calibration and performance assessment of an innovative high-temperature cavitometer*. Sens. Actuators Phys., 240, 57–69.

[17] Minnaert, M. (1933) *XVI.* On musical air-bubbles and the sounds of running water. Lond. Edinb. Dublin Philos. Mag. J. Sci., 16 (104), 235–248.

[18] Tzanakis, I., Lebon, G.S.B., Eskin, D.G., and Pericleous, K. (2016) *Investigation of the factors influencing cavitation intensity during the ultrasonic treatment of molten aluminium*. Mater. Des., 90, 979–983.

[19] Lebon, G.S.B., Tzanakis, I., Pericleous, K., and Eskin, D. (2018) *Experimental and numerical investigation of acoustic pressures in different liquids*. Ultrason. Sonochem., 42, 411–421.

[20] Eskin, D.G., Tzanakis, I., Wang, F., Lebon, G.S.B., Pericleous, K., Lee, P.D., Connolley, T., and Mi, J. (2017) *Fundamental studies of ultrasonic melt processing*. Proc. 6th Decenn. Int. Conf. Solidif. Process., 546–549.

[21] Nowak, T., Cairós, C., Batyrshin, E., and Mettin, R. (2015) *Acoustic streaming and bubble translation at a cavitating ultrasonic horn*. 020002.

[22] Yasui, K., Iida, Y., Tuziuti, T., Kozuka, T., and Towata, A. (2008) *Strongly interacting bubbles under an ultrasonic horn*. Phys. Rev. E, 77 (1).

[23] Tzanakis, I., Lebon, G.S.B., Eskin, D.G., and Pericleous, K.A. (2017) *Characterizing the cavitation development and acoustic spectrum in various liquids*. Ultrason. Sonochem., 34, 651–662.

[24] Schnerr, G.H., and Sauer, J. (2001) *Physical and Numerical Modeling of Unsteady Cavitation Dynamics*. Proc. 4th Int. Conf. Multiph. Flow, 1.

[25] Weller, H.G. (2017) *OpenFOAM*, OpenCFD Ltd (ESI Group).

[26] Yoshizawa, A. (1986) *Statistical theory for compressible turbulent shear flows, with the application to subgrid modeling*. Phys. Fluids, 29 (7), 2152.